

Higgs boson decays $h \rightarrow MZ$ in the TNMSSM

Huai-Cong Hu^{1*}, Zhao-Yang Zhang^{1†}, Ning-Yu Zhu^{1‡}, Hai-Xiang Chen^{1§}

¹*School of Physical Science and Technology,
Guangxi University, Nanning, 530004, China*

Abstract

We study the SM-like Higgs boson decays $h \rightarrow MZ$ in the Triplet extended NMSSM (TNMSSM), where M is a vector meson ($\rho, \omega, \phi, J/\Psi, \Upsilon$). Compared to the minimal supersymmetric standard model (MSSM), the TNMSSM includes two new SU(2) triplets with hypercharge ± 1 and a SM gauge singlet which are coupled to each other. The indirect contributions to the decays $h \rightarrow MZ$ are produced from the effective $h\gamma Z$ vertex, and they are more important than the direct contributions. The results of this work would encourage a detection on $h \rightarrow Z\gamma$ at the future high energy colliders for exploring new physics beyond the SM.

PACS numbers:

Keywords: Supersymmetry, Higgs boson decay

* huaiconghu@163.com

† 1311274306@qq.com

‡ hnzhu@163.com

§ haixchen@hotmail.com

I. INTRODUCTION

Since the Higgs was discovered by the ATLAS and CMS collaborations in 2012[1, 2], many questions regarding its properties remain unanswered. According to the latest experimental data the measured mass of the Higgs boson is[3].

$$m_h = 125.25 \pm 0.17 \text{ GeV}$$

As a new elementary particle, h is largely consistent with the neutral Higgs boson predicted by the SM. However many questions have been raised that challenge the SM framework.

Weak scale supersymmetry (SUSY) is a promising extension of the Standard Model (SM): it naturally explains why the electroweak (EW) symmetry breaking scale is much smaller than the Planck scale, and solve the gauge hierarchy problem[4, 5]. But, minimum supersymmetric SM (MSSM) cannot fully solve the hierarchy problem. And it has another problem named “the μ problem”. Hence, extensions of the MSSM have been proposed to solve these problems. For example the extension of the MSSM by adding a (SM) gauge singlet which is coupled to Higgs doublets (the NMSSM) has been proposed to solve the μ problem.

But unfortunately the NMSSM with all the couplings being perturbative up to the GUT scale also does not really solve the little hierarchy problem[6–9]. If taking little hierarchy problem seriously, then one should consider another source of Higgs quadruple coupling, which will not decouple in the large $\tan \beta$ limit[10]. The model which extended of the MSSM by adding SU(2) triplets(TMSSM)[11–13] possess such a Higgs quartic coupling naturally.

Combined the advantages of the NMSSM and the TNMSSM, they can solve each other’s problems[10]. In the triplet extended NMSSM (TNMSSM), the singlet interactions do not play any important role in raising the physical Higgs mass: one rely on triplets instead in achieving this goal. So, one also do not face the usual little hierarchy problems of the NMSSM.

In our work, we study 125 GeV SM-like Higgs boson decay $h \rightarrow MZ$ in the framework of the TNMSSM, with M representing the mesons ρ , ω , ϕ , J/ψ and Υ . The decay of $h \rightarrow MZ$ have been shown in[14–20], via the effective vertex $hZ\gamma^*$. Subsequent transition to $\gamma^* \rightarrow M$. There is no $hZ\gamma$ coupling at tree level, but it can be contributed by loop diagram[14]. The

first evidence for the process $h \rightarrow \gamma Z$ is presented by the ATLAS and CMS. The observed signal strength at the 68% confidence level is $\mu = 2.2_{-0.9}^{+1.0}$ for ATLAS analysis, $\mu = 2.4_{-0.9}^{+1.0}$ for the CMS analysis, and $\mu = 2.2 \pm 0.7$ for their combination[21]. Due to the process $h \rightarrow \gamma Z$ had observed and the results are shifted from the SM. This presupposes the existence of a new physics, whose contribution to the process may be able to explain the deviations between observed decays and SM predictions, and thus the associated decay process deserves to be investigated. This coupling is important for probing new physics. In the TNMSSM, there are additional coupling of the Higgs boson to additional charged scalars and charged fermions. They contribute to the $hZ\gamma$ coupling by loop diagrams.

The paper is organized as follows. we briefly present the main ingredients of the TNMSSM in Sec. II. We give the Higgs boson decays $h \rightarrow Z\gamma$ and $h \rightarrow MZ$ formulas in Sec. III. We show the input parameters and numerical results in Sec. IV. In the last section we give the discussion and conclusion. Finally, some relate formulas are shown in Appendix.

II. THE TNMSSM

Compared to the MSSM, the TNMSSM includes two new $SU(2)_L$ triplet superfields T, \bar{T} with hypercharge ± 1 and a SM gauge singlet superfield \hat{s} which are coupled to each other.

The superpotential of the TNMSSM can be written as:

$$W = -Y_d \hat{d} \hat{q} \hat{H}_d - Y_e \hat{e} \hat{l} \hat{H}_d + \chi_d \hat{H}_d \hat{T} \hat{H}_d + \lambda \hat{H}_u \hat{H}_d \hat{s} + \chi_t \hat{H}_u \hat{\bar{T}} \hat{H}_u + \frac{1}{3} \kappa \hat{s}^3 + \Lambda_T \hat{s} \hat{\bar{T}} \hat{T} + Y_u \hat{u} \hat{q} \hat{H}_u$$

Here the triplet superfields with hypercharge $Y = \pm 1$ are defined as:

$$T \equiv T^a \sigma^a = \begin{pmatrix} T^+/\sqrt{2} & -T^{++} \\ T^0 & -T^+/\sqrt{2} \end{pmatrix}$$

$$\bar{T} \equiv \bar{T}^a \sigma^a = \begin{pmatrix} \bar{T}^-/\sqrt{2} & -\bar{T}^0 \\ \bar{T}^{--} & -\bar{T}^-/\sqrt{2} \end{pmatrix}$$

The soft SUSY breaking terms are shown as the follow

$$\begin{aligned}
-\mathcal{L}_{\text{soft}} = & \frac{1}{2}(M_1\lambda_1\lambda_1 + M_2\lambda_2\lambda_2 + M_3\lambda_3\lambda_3 + h.c.) + m_{H_u}^2|H_u|^2 + m_{H_d}^2|H_d|^2 + m_T^2\text{Tr}(\bar{T}^\dagger T) + \\
& m_T^2\text{Tr}(T^\dagger T) + m_S^2|S|^2 + m_{\tilde{Q}}^2|\tilde{Q}|^2 + m_{\tilde{u}}^2|\tilde{u}_R|^2 + m_{\tilde{d}}^2|\tilde{d}_R|^2 + m_{\tilde{l}}^2|\tilde{l}|^2 + m_{\tilde{e}}^2|\tilde{e}_R|^2 + \\
& (T_{\Lambda T}\text{tr}(T\bar{T})S + T_{\chi d}H_d \cdot TH_d + T_{\chi t}H_u \cdot \bar{T}H_u + \frac{T_\kappa}{3}S^3 + T_\lambda H_u \cdot H_d S + \\
& T_d H_d \cdot \tilde{Q}d^* - T_u H_u \cdot \tilde{Q}u^* + T_e H_d \cdot Le^* + h.c.), \tag{1}
\end{aligned}$$

where the respective definitions of the products between two $SU(2)_L$ doublets and between a $SU(2)_L$ doublets and a $SU(2)_L$ triplet are given as follows:

$$\begin{aligned}
H_u \cdot H_d &= H_u^+ H_d^- - H_u^0 H_d^0, \\
H_u \cdot \bar{T}H_u &= \sqrt{2}H_u^0 H_u^+ \bar{T}^- - (H_u^0)^2 \bar{T}^0 - (H_u^+)^2 \bar{T}^{--}, \\
H_d \cdot TH_d &= \sqrt{2}H_d^0 H_d^- T^+ - (H_d^0)^2 T^0 - (H_d^-)^2 T^{++}.
\end{aligned}$$

Once the electroweak symmetry is spontaneously broken, the neutral scalar fields can be define as

$$\begin{aligned}
\langle H_u^0 \rangle &= \frac{v_u + \phi_u + i\sigma_u}{\sqrt{2}}, & \langle H_d^0 \rangle &= \frac{v_d + \phi_d + i\sigma_d}{\sqrt{2}}, \\
\langle T^0 \rangle &= \frac{v_T + \phi_T + i\sigma_T}{\sqrt{2}}, & \langle \bar{T}^0 \rangle &= \frac{\bar{v}_T + \phi_{\bar{T}} + i\sigma_{\bar{T}}}{\sqrt{2}}, \\
\langle S \rangle &= \frac{v_s + \phi_s + i\sigma_s}{\sqrt{2}}.
\end{aligned}$$

and we define the ratio v_u to v_d as $\tan \beta = \frac{v_u}{v_d}$ the ratio v_T to $v_{\bar{T}}$ as $\tan \beta' = \frac{v_T}{v_{\bar{T}}}$.

Since we introduce a single state and two triplet states, we have five minimization equations, including the usual upper and lower Higgs. In general, the vacuum expectation value of the triplet states must be small to avoid large ρ -parameter corrections[10].

In the basis $(H_d^-, H_u^{+,*}, \bar{T}^-, T^{+,*})$ and $(H_d^{-,*}, H_u^+, \bar{T}^{-,*}, T^+)$, the definition of the mass squared matrix for charged Higgs is given by

$$m_{H^\pm}^2 = \begin{pmatrix} m_{H_d^-, H_d^{-,*}} & m_{H_u^{+,*}, H_d^{-,*}}^* & m_{\bar{T}^-, H_d^{-,*}}^* & m_{T^{+,*}, H_d^{-,*}}^* \\ m_{H_d^-, H_u^+} & m_{H_u^{+,*}, H_u^+} & m_{\bar{T}^-, H_u^+}^* & m_{T^{+,*}, H_u^+}^* \\ m_{H_d^-, \bar{T}^{-,*}} & m_{H_u^{+,*}, \bar{T}^{-,*}} & m_{\bar{T}^-, \bar{T}^{-,*}} & m_{T^{+,*}, \bar{T}^{-,*}}^* \\ m_{H_d^-, T^+} & m_{H_u^{+,*}, T^+} & m_{\bar{T}^-, T^+} & m_{T^{+,*}, T^+} \end{pmatrix} \tag{2}$$

where

$$\begin{aligned}
m_{H_d^-, H_d^{-,*}} &= \frac{1}{2}v_s^2|\lambda|^2 + \frac{1}{8}[g_1^2(2v_{\bar{T}}^2 - 2v_T^2 - v_u^2 + v_d^2) + g_2^2(-2v_{\bar{T}}^2 + 2v_T^2 + v_d^2 + v_u^2)] + v_d^2|\chi_d|^2 + m_{H_d}^2, \\
m_{H_d^-, H_u^+} &= \frac{1}{2}[\lambda(-v_d v_u \lambda^* + v_s^2 \kappa^* - v_T v_{\bar{T}} \Lambda_T^*) + \sqrt{2}v_s T_\lambda] + \frac{1}{4}g_2^2 v_d v_u, \\
m_{H_u^{+,*}, H_u^+} &= \frac{1}{2}v_s^2|\lambda|^2 + \frac{1}{8}[(g_1^2 + g_2^2)v_u^2 - (-g_2^2 + g_1^2)(2v_{\bar{T}}^2 - 2v_T^2 + v_d^2)] + v_u^2|\chi_t|^2 + m_{H_u}^2, \\
m_{H_d^-, \bar{T}^{-,*}} &= \frac{1}{2\sqrt{2}}g_2^2 v_d v_{\bar{T}} - \frac{1}{\sqrt{2}}v_s(v_d \chi_d \Lambda_T^* + v_u \lambda \chi_t^*), \\
m_{H_u^{+,*}, \bar{T}^{-,*}} &= \frac{1}{2\sqrt{2}}g_2^2 v_{\bar{T}} v_u + \frac{1}{\sqrt{2}}(-2v_{\bar{T}} v_u \chi_t + v_d v_s \lambda) \chi_t^* - v_u T_{\chi, t^*}, \\
m_{\bar{T}^-, \bar{T}^{-,*}} &= \frac{1}{2}v_s^2|\Lambda_T|^2 + \frac{1}{4}[2g_2^2 v_{\bar{T}}^2 + (g_1^2 2v_{\bar{T}}^2 - 2v_T^2 - v_u^2 + v_d^2)] + v_u^2|\chi_t|^2 + m_{\bar{T}}^2, \\
m_{H_d^-, T^+} &= \frac{1}{2\sqrt{2}}g_2^2 v_d v_T + \frac{1}{\sqrt{2}}v_s v_u \chi_d \lambda^* - v_d(\sqrt{2}v_T |\chi_d|^2 + T_{\chi_d}), \\
m_{H_u^{+,*}, T^+} &= \frac{1}{2\sqrt{2}}g_2^2 v_d v_u - \frac{1}{\sqrt{2}}v_s(\Lambda_T v_u \chi_t^* + v_d \chi_d \lambda^*), \\
m_{\bar{T}^-, T^+} &= \frac{1}{2}g_2^2 v_T v_{\bar{T}} + \frac{1}{2}[\Lambda_T(-v_d v_u \lambda^* + v_s^2 \kappa^* - v_T v_{\bar{T}} \Lambda_T^*) + \sqrt{2}v_s T_{\Lambda_T}], \\
m_{T^{+,*}, T^+} &= \frac{1}{2}v_s|\Lambda_T|^2 + \frac{1}{4}[2g_2^2 v_T^2 + g_1(-2v_{\bar{T}}^2 + 2v_T^2 - v_d^2 + v_u^2)] + v_d^2|\chi_d|^2 + m_T^2.
\end{aligned}$$

This matrix is diagonalized by Z^+ :

$$Z^+ m_H^2 Z^{+, \dagger} = m_{2, H^-}^{\text{dia}}$$

with

$$H_d^- = \sum_j Z_{j1}^+ H_j^-, \quad H_u^+ = \sum_j Z_{j2}^+ H_j^+, \quad T^- = \sum_j Z_{j3}^+ H_j^-, \quad T^+ = \sum_j Z_{j4}^+ H_j^+.$$

The mass of the SM-like Higgs boson in the TNMSSM can be written as:

$$m_h = \sqrt{(m_{h_1}^0)^2 + \Delta m_h^2} \quad (3)$$

where $m_{h_1}^0$ is the lightest tree-level Higgs boson mass, and Δm_h^2 is the radiative correction.

The two-loop leading-log radiative corrections can be given as:

$$\Delta m_h^2 = \frac{3m_t^4}{4\pi^2 v^2} \left[\left(\tilde{t} + \frac{1}{2} \tilde{X}_t \right) + \frac{1}{16\pi^2} \left(\frac{3m_t^2}{2v^2} - 32\pi\alpha_3 \right) (\tilde{t}^2 + \tilde{X}_t \tilde{t}) \right] \quad (4)$$

$$\tilde{t} = \log \frac{M_S^2}{m_t^2}, \quad \tilde{X}_t = \frac{2\tilde{A}_t^2}{M_S^2} \left(1 - \frac{\tilde{A}_t^2}{12M_S^2} \right) \quad (5)$$

where α_3 is the running strong coupling constant, $M_S = \sqrt{m_{\tilde{t}_1} m_{\tilde{t}_2}}$ with $m_{\tilde{t}_{1,2}}$ are the stop masses. $\tilde{A}_t = A_t - \mu \cot \beta$ with $A_t = T_{u,33}/Y_{u,33}$.

III. ANALYTICAL FORMULA

In this section we discuss the Higgs boson decay processes $h \rightarrow Z\gamma$ and $h \rightarrow MZ$. The dominating Feynman diagrams for $h \rightarrow MZ$ are shown in Fig.1. The first two diagrams in Fig.1 are the direct contributions, and the last two diagrams represent the indirect contributions. For the indirect contribution, there is a process $h \rightarrow Z\gamma^* \rightarrow MZ$, where γ^* is off-shell and changes into the final state meson.

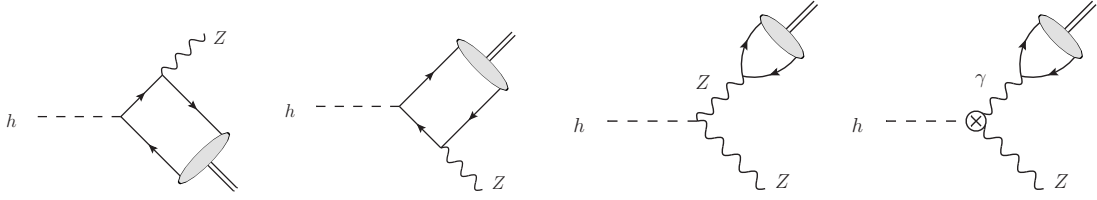


FIG. 1: The diagrams contributing to the decay $h \rightarrow MZ$. The crossed circle in the last graph represents the effective vertex $h \rightarrow Z\gamma^*$ from the one loop diagrams.

There is no contribution to $hZ\gamma$ coupling at tree level in the TNMSSM, but it can be created by loop diagrams. The $h \rightarrow Z\gamma^*$ process can be used to probe for New Physics. So we will focus on discussing $h \rightarrow Z\gamma^*$. In the TNMSSM, the non-standard $h^0\gamma Z$ vertex should be taken into account. The effective Lagrangian for $h\gamma Z$ is written as:

$$\mathcal{L}_{eff} = \frac{\alpha}{4\pi v} \left(\frac{2C_{\gamma Z}}{s_W c_W} h F_{\mu\nu} Z^{\mu\nu} - \frac{2\tilde{C}_{\gamma Z}}{s_W c_W} h F_{\mu\nu} \tilde{Z}^{\mu\nu} \right), \quad (6)$$

with $s_W = \sin\theta_W, c_W = \cos\theta_W$. The decay width of $h \rightarrow Z\gamma$ deduced by the effective Lagrangian defined in Eq.(6) is:

$$\Gamma(h \rightarrow Z\gamma) = \frac{\alpha^2 m_{h^0}^3}{32\pi^3 v^2 s_W^2 c_W^2} \left(1 - \frac{m_Z^2}{m_{h^0}^2}\right)^3 (|C_{\gamma Z}|^2 + |\tilde{C}_{\gamma Z}|^2). \quad (7)$$

The loop diagrams make additional contributions to $h \rightarrow MZ$ decays in new physics. And the decay width of $h \rightarrow MZ$ is given by:

$$\begin{aligned} \Gamma(h \rightarrow MZ) &= \frac{m_{h^0}^3}{4\pi v^4} \lambda^{1/2}(1, r_Z, r_M) (1 - r_Z - r_M)^2 \\ &\times \left[|F_{\parallel}^{MZ}|^2 + \frac{8r_M r_Z}{(1 - r_Z - r_M)^2} \left(|F_{\perp}^{MZ}|^2 + |\tilde{F}_{\perp}^{MZ}|^2 \right) \right], \quad (8) \end{aligned}$$

with $\lambda(x, y, z) = (x - y - z)^2 - 4yz$, $r_Z = \frac{m_Z^2}{m_h^2}$ and $r_M = \frac{m_M^2}{m_h^2}$, m_M is the mass of vector meson. F_{\parallel}^{MZ} and F_{\perp}^{MZ} represent the CP-even longitudinal and transverse form factors, respectively \tilde{F}_{\perp}^{MZ} represent the CP-odd transverse form factors. For the vector mesons considered in this work, the mass ratio r_M is very small, but it can make significant contributions to the transverse polarization states. In order to obtain better results we keep them in our study.

In Eq.(8), F_{\parallel}^{MZ} , F_{\perp}^{MZ} and \tilde{F}_{\perp}^{MZ} could be divided into direct and indirect parts. The indirect contributions are shown as follows:

$$F_{\parallel \text{indirect}}^{MZ} = \frac{\kappa_Z}{1 - r_M/r_Z} \sum_q f_M^q v_q + C_{\gamma Z} \frac{\alpha_s(m_M)}{4\pi} \frac{4r_Z}{1 - r_Z - r_M} \sum_q f_M^q Q_q, \quad (9)$$

$$F_{\perp \text{indirect}}^{MZ} = \frac{\kappa_Z}{1 - r_M/r_Z} \sum_q f_M^q v_q + C_{\gamma Z} \frac{\alpha_s(m_M)}{4\pi} \frac{1 - r_Z - r_M}{r_M} \sum_q f_M^q Q_q, \quad (10)$$

$$\tilde{F}_{\perp \text{indirect}}^{MZ} = \tilde{C}_{\gamma Z} \frac{\alpha_s(m_M)}{4\pi} \frac{\lambda^{1/2}(1, r_Z, r_M)}{r_M} \sum_q f_M^q Q_q, \quad (11)$$

where $v_q = \frac{T_3^q}{2} - Q_q \sin^2 \theta_W$ are the vector couplings of the Z boson to the quark q , κ_Z is the ratio of the coupling of the SM-like Higgs boson to Z boson to the corresponding SM value. α_s is the strong coupling constant. The flavor-specific decay constants f_M^q are defined by

$$\langle M(k, \varepsilon) | \bar{q} \gamma^\mu q | 0 \rangle = -i f_M^q m_M \varepsilon^{*\mu}, \quad q = u, d, s \dots \quad (12)$$

The calculations can be simplified by the following relationship

$$\sum_q f_M^q Q_q = f_M Q_M, \quad \sum_q f_M^q v_q = f_M v_M. \quad (13)$$

The vector meson decay constants f_M, Q_M, v_M are shown in Table I.

The concrete forms of $C_{\gamma Z}$ and $\tilde{C}_{\gamma Z}$ in Eqs. (9-11) can be written as[16, 17, 22]

$$\begin{aligned} C_{\gamma Z} &= C_{\gamma Z}^{SM} + C_{\gamma Z}^{NP}, & \tilde{C}_{\gamma Z} &= \tilde{C}_{\gamma Z}^{SM} + \tilde{C}_{\gamma Z}^{NP}. \\ C_{\gamma Z}^{SM} &= \sum_q \frac{2N_c Q_q v_q}{3} A_f(\tau_q, r_Z) + \sum_l \frac{2Q_l v_l}{3} A_f(\tau_l, r_Z) - \frac{1}{2} A_W^{\gamma Z}(\tau_W, r_Z), \\ \tilde{C}_{\gamma Z}^{SM} &= \sum_q \tilde{\kappa}_q N_c Q_q v_q B_f(\tau_q, r_Z) + \sum_l \tilde{\kappa}_l Q_l v_l B_f(\tau_l, r_Z), \end{aligned} \quad (14)$$

where $\tau_i = \frac{4m_i^2}{m_h^2}$, v_l are the vector couplings of the Z boson to the leptons are the vector couplings of the Z boson to the leptons and Q_l represent the charge of leptons. $C_{\gamma Z}^{SM}$ and $\tilde{C}_{\gamma Z}^{SM}$

Vector meson	ω	ρ	ϕ	J/ψ	Υ
m_M/GeV	0.782	0.77	1.02	3.097	9.46
f_M/GeV	0.194	0.216	0.223	0.403	0.684
v_M	$-\frac{\sin^2\theta_W}{3\sqrt{2}}$	$\frac{1}{\sqrt{2}}(\frac{1}{2} - \sin^2\theta_W)$	$-\frac{1}{4} + \frac{\sin^2\theta_W}{3}$	$\frac{1}{4} - \frac{2\sin^2\theta_W}{3}$	$-\frac{1}{4} + \frac{\sin^2\theta_W}{3}$
Q_M	$\frac{1}{3\sqrt{2}}$	$\frac{1}{\sqrt{2}}$	$-\frac{1}{3}$	$\frac{2}{3}$	$-\frac{1}{3}$
$f_M^\perp/f_M = f_M^{q\perp}/f_M^q$	0.71	0.72	0.76	0.91	1.09

TABLE I: The mesons decay constants f_M , Q_M , v_M will be used in the numerical analysis, where f_M^\perp and $f_M^{q\perp}$ represent the transverse decay constants and the flavor-specific transverse decay constants.

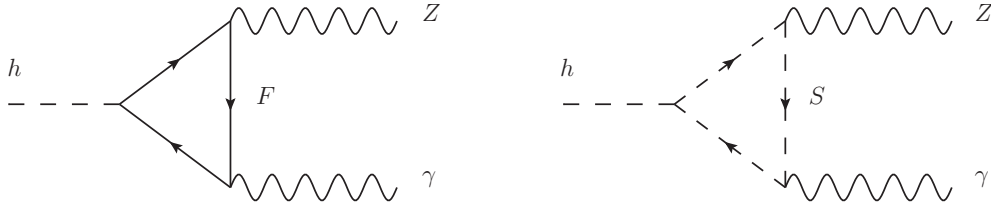


FIG. 2: The one loop diagrams for $h \rightarrow \gamma Z$ in the TNMSSM, with $F = \chi^\pm, \chi^{\pm\pm}$ denoting the charged fermions and $S = \tilde{u}_i^+, \tilde{d}_i^-, S_\alpha^\pm, S_\alpha^{\pm\pm}$ denoting the squarks and charged scalars.

represent the SM contributions to $h \rightarrow Z\gamma$. $\tilde{\kappa}_q$ and $\tilde{\kappa}_l$ represent the effective Higgs couplings to the quarks and the leptons. A_f , B_f , and $A_W^{\gamma Z}$ are loop function could find in Refs. [18, 27]. The numerical values of $C_{\gamma Z}^{\text{SM}}$ and $\tilde{C}_{\gamma Z}^{\text{SM}}$ are taken as : $C_{\gamma Z}^{\text{SM}} \sim -2.395 + 0.001i$, $\tilde{C}_{\gamma Z}^{\text{SM}} \sim 0$ in Ref. [16].

In the TNMSSM, the one loop diagrams contributing to $h \rightarrow \gamma Z$ are shown in Fig.2, where F represent the charged Fermions and S represent the charged scalars. The new contributions to $C_{\gamma Z}$ originate from the exchanged particles:charginos, sleptons, squarks, and charged Higgs.

The CP-odd coupling $\tilde{C}_{\gamma Z}$ is 0 in the SM. In the TNMSSM, the $h\gamma Z$ coupling can be written as $\bar{F}_1 i(A + B\gamma^5)F_2 h$, where A is the CP-even part and B is the CP-odd part[16, 17]. For interaction $\bar{F}_1 i(C^R P_R + C^L P_L)F_2 h$ with $P_L = \frac{1-\gamma_5}{2}$ and $P_R = \frac{1+\gamma_5}{2}$, the CP-even part is

$A = \frac{1}{2}(C^L + C^R)$ and the CP-odd part is $B = \frac{1}{2}(C^R - C^L)$. In the TNMSSM,

$$\begin{aligned} C_{hS^+S^-}^L &= C_{hS^+S^-}^R, & C_{hS^{++}S^{--}}^L &= C_{hS^{++}S^{--}}^R, & C_{h\tilde{f}\tilde{f}}^L &= C_{h\tilde{f}\tilde{f}}^R, \\ C_{h\chi^+\chi^-}^L &= C_{h\chi^+\chi^-}^R, & C_{h\chi^{++}\chi^{--}}^L &= C_{h\chi^{++}\chi^{--}}^R \end{aligned}$$

and only $C_{Z\chi^+\chi^-}^L \neq C_{Z\chi^+\chi^-}^R$ or $C_{Z\chi^{++}\chi^{--}}^L \neq C_{Z\chi^{++}\chi^{--}}^R$. But $C_{Z\chi^+\chi^-}^L + C_{Z\chi^+\chi^-}^R \gg C_{Z\chi^+\chi^-}^R - C_{Z\chi^+\chi^-}^L$, $C_{Z\chi^{++}\chi^{--}}^L + C_{Z\chi^{++}\chi^{--}}^R \gg C_{Z\chi^{++}\chi^{--}}^R - C_{Z\chi^{++}\chi^{--}}^L$. So we can neglect the CP-odd coupling $\tilde{C}_{\gamma Z}^{NP}$ in the TNMSSM. The expression of CP-even coupling $C_{\gamma Z}^{NP}$ in the TNMSSM is:

$$\begin{aligned} C_{\gamma Z}^{NP} &= \frac{c_w}{2} \left[\sum_{S^\pm} (2c_w^2 - 1) g_{hS^+S^-} (m_Z^2/m_{S^\pm}^2) A_0[x_{S^\pm}, \lambda_{S^\pm}] \right. \\ &+ \sum_{S^{\pm\pm}} (2c_w^2 - 1) g_{hS^{++}S^{--}} (m_Z^2/m_{S^{\pm\pm}}^2) A_0[x_{S^{\pm\pm}}, \lambda_{S^{\pm\pm}}] \\ &+ \sum_{\tilde{f}} N_c Q_{\tilde{f}} \hat{v}_{\tilde{f}} g_{h\tilde{f}\tilde{f}} (m_Z^2/m_{\tilde{f}}^2) A_0[x_{\tilde{f}}, \lambda_{\tilde{f}}] \\ &+ \sum_{\chi^\pm; m,n=L,R} g_{h\chi^\pm\chi^\mp}^m g_{Z\chi^\pm\chi^\mp}^n (2m_W/m_{\chi^\pm}) A_{1/2}[x_{\chi^\pm}, \lambda_{\chi^\pm}] \\ &+ \left. \sum_{\chi^{\pm\pm}; m,n=L,R} g_{h\chi^{\pm\pm}\chi^{\mp\mp}}^m g_{Z\chi^{\pm\pm}\chi^{\mp\mp}}^n (2m_W/m_{\chi^{\pm\pm}}) A_{1/2}[x_{\chi^{\pm\pm}}, \lambda_{\chi^{\pm\pm}}] \right] \quad (15) \end{aligned}$$

where $x_i = 4m_i^2/m_h^2$, $\lambda_i = 4m_i^2/m_Z^2$, $\hat{v}_{\tilde{f}_1} = (T_3^f \cos^2 \theta_f - Q_f s_w^2)/c_w$, $\hat{v}_{\tilde{f}_2} = (T_3^f \sin^2 \theta_f - Q_f s_w^2)/c_w$, $\hat{v}_{\tilde{f}_1}$ and $\hat{v}_{\tilde{f}_2}$ represent up and down-quark sectors, T_3^f is the weak isospin of fermion f , θ_f is the mixing angle of sfermions $\tilde{f}_{1,2}$. The function A_0 , $A_{1/2}$ can be found at [27, 28]. The concrete expressions of couplings

$$\begin{aligned} g_{hS^+S^-} &= -\frac{v}{2m_Z^2} C_{hS^+S^-}^{L,R}, & g_{hS^{++}S^{--}} &= -\frac{v}{2m_Z^2} C_{hS^{++}S^{--}}^{L,R} \\ g_{h\tilde{f}\tilde{f}} &= -\frac{v}{2m_Z^2} C_{h\tilde{f}\tilde{f}}^{L,R}, & g_{h\chi^\pm\chi^\mp}^{L,R} &= -\frac{1}{e} C_{h\chi^\pm\chi^\mp}^{L,R} \\ g_{Z\chi^\pm\chi^\mp}^{L,R} &= -\frac{1}{e} C_{Z\chi^\pm\chi^\mp}^{L,R}, & g_{h\chi^{\pm\pm}\chi^{\mp\mp}}^{L,R} &= -\frac{1}{e} C_{h\chi^{\pm\pm}\chi^{\mp\mp}}^{L,R} \\ g_{Z\chi^{\pm\pm}\chi^{\mp\mp}}^{L,R} &= -\frac{1}{e} C_{Z\chi^{\pm\pm}\chi^{\mp\mp}}^{L,R}. \end{aligned}$$

As discussed in Ref.[23], the QCD corrections to the process $h \rightarrow Z\gamma$ are around 0.1% which medicates the QCD corrections can be neglected safely. In other words, we can safely neglect QCD corrections because they are very small.

Compared to the indirect contributions, the direct contributions are very different, and they can be calculated in a power series $(m_q/m_h)^2$ or $(\Lambda_{QCD}/m_h)^2$. For the transversely polarized vector meson, leading-twist projections provide direct contributions. We can get the direct contributions by the asymptotic function $\phi_M^\perp = 6x(1-x)$ [24–26]

$$F_{\perp\text{direct}}^{MZ} = \sum_q f_M^{q\perp} v_q \kappa_q \frac{3m_q}{2m_M} \frac{1 - r_Z^2 + 2r_Z \ln r_Z}{(1 - r_Z)^2} \quad (16)$$

$$\tilde{F}_{\perp\text{direct}}^{MZ} = \sum_q f_M^{q\perp} v_q \tilde{\kappa}_q \frac{3m_q}{2m_M} \frac{1 - r_Z^2 + 2r_Z \ln r_Z}{(1 - r_Z)^2} \quad (17)$$

In the calculations, it is found that the direct contribution is much smaller than the indirect contribution. Which indicates that the indirect contributions are more important than the direct contributions. The contributions for the decay width of $h \rightarrow MZ$ in SM are shown in Table II.

	ρ	ω	ϕ	J/ ψ	Υ
$F_{\parallel\text{ind}}^{MZ}$	0.0423 $+4.3 \times 10^{-4} C_{\gamma Z}^{SM}$	-0.0102 $+1.3 \times 10^{-4} C_{\gamma Z}^{SM}$	-0.0392 $-2.1 \times 10^{-4} C_{\gamma Z}^{SM}$	0.041 $+7.5 \times 10^{-4} C_{\gamma Z}^{SM}$	-0.115 $-6.1 \times 10^{-4} C_{\gamma Z}^{SM}$
$F_{\perp\text{ind}}^{MZ}$	0.042 $+1.181 C_{\gamma Z}^{SM}$	-0.01 $+0.343 C_{\gamma Z}^{SM}$	-0.039 $-0.327 C_{\gamma Z}^{SM}$	0.04 $+0.128 C_{\gamma Z}^{SM}$	-0.12 $-0.011 C_{\gamma Z}^{SM}$
$F_{\perp\text{direct}}^{MZ}$	0.0037	-0.00087	-0.00257	-0.00088	-0.00080

TABLE II: The contributions for the decay width of $h \rightarrow MZ$ in SM, with $C_{\gamma Z}^{SM} \simeq -2.43$.

Normalized to the SM expectation, the signal strengths for the Higgs decay channels can be quantified as

$$\mu_{MZ}^{ggF} = \frac{\sigma_{\text{NP}}(ggF) Br_{\text{NP}}(h \rightarrow MZ)}{\sigma_{\text{SM}}(ggF) Br_{\text{SM}}(h \rightarrow MZ)} \quad (18)$$

$$\mu_{\gamma\gamma}^{ggF} = \frac{\sigma_{\text{NP}}(ggF) Br_{\text{NP}}(h \rightarrow \gamma\gamma)}{\sigma_{\text{SM}}(ggF) Br_{\text{SM}}(h \rightarrow \gamma\gamma)} \quad (19)$$

where ggF stands for gluon-gluon fusion. And Higgs production cross sections can be written as

$$\frac{\sigma_{\text{NP}}(ggF)}{\sigma_{\text{SM}}(ggF)} \approx \frac{\Gamma_{\text{NP}}(h \rightarrow gg)}{\Gamma_{\text{SM}}(h \rightarrow gg)} \quad (20)$$

Through Eqs.(18-20), the signal strengths for $h \rightarrow MZ$ and $h \rightarrow \gamma\gamma$ can be quantified as

$$\mu_{MZ}^{ggF} \approx \frac{\Gamma_{\text{NP}}(h \rightarrow gg)\Gamma_{\text{NP}}(h \rightarrow MZ)/\Gamma_{\text{NP}}^h}{\Gamma_{\text{SM}}(h \rightarrow gg)\Gamma_{\text{SM}}(h \rightarrow MZ)/\Gamma_{\text{SM}}^h} = \frac{\Gamma_{\text{NP}}(h \rightarrow gg)\Gamma_{\text{NP}}(h \rightarrow MZ)\Gamma_{\text{SM}}^h}{\Gamma_{\text{SM}}(h \rightarrow gg)\Gamma_{\text{SM}}(h \rightarrow MZ)\Gamma_{\text{NP}}^h} \quad (21)$$

$$\mu_{\gamma\gamma}^{ggF} \approx \frac{\Gamma_{\text{NP}}(h \rightarrow gg)\Gamma_{\text{NP}}(h \rightarrow \gamma\gamma)/\Gamma_{\text{NP}}^h}{\Gamma_{\text{SM}}(h \rightarrow gg)\Gamma_{\text{SM}}(h \rightarrow \gamma\gamma)/\Gamma_{\text{SM}}^h} = \frac{\Gamma_{\text{NP}}(h \rightarrow gg)\Gamma_{\text{NP}}(h \rightarrow \gamma\gamma)\Gamma_{\text{SM}}^h}{\Gamma_{\text{SM}}(h \rightarrow gg)\Gamma_{\text{SM}}(h \rightarrow \gamma\gamma)\Gamma_{\text{NP}}^h} \quad (22)$$

where Γ_{NP}^h and Γ_{SM}^h denote total decay widths in the NP model and the SM respectively.

IV. NUMERICAL ANALYSIS

In this section, we discuss the numerical results of the Higgs boson decays $h \rightarrow MZ$ in the TNMSSM are present. The results are constrained by the SM-like Higgs boson mass in the TNMSSM with $124.74 \text{ GeV} \leq m_h \leq 125.76 \text{ GeV}$, where a 3σ experimental error is considered. For the SM parameters, we take $m_W = 80.385 \text{ GeV}$, $m_Z = 91.1876 \text{ GeV}$, $m_u = 2.16 \text{ MeV}$, $m_d = 4.67 \text{ MeV}$, $m_s = 93.4 \text{ MeV}$, $m_c = 1.27 \text{ GeV}$, $m_b = 4.18 \text{ GeV}$, $m_t = 172.69 \text{ GeV}$. For the squark sector, we take $m_{\tilde{Q}} = m_{\tilde{u}} = m_{\tilde{d}} = \text{diag}(M_Q, M_Q, M_Q)$ and $T_{u,d} = Y_{u,d} \text{diag}(A_Q, A_Q, A_t)$ for simplicity. According to the latest experimental data [3], We take $M_Q = 2 \text{ TeV}$, $A_Q = 1.5 \text{ TeV}$. And for the slepton sector, we take $m_{\tilde{l}} = m_{\tilde{e}} = 2 \text{ TeV}$, $T_e = Y_e \text{diag}(A_e, A_e, A_e)$ and $A_e = 1.5 \text{ TeV}$. Then we take $\mu = 1 \text{ TeV}$, $\tan \beta = 8$, $\tan \beta' = 10$, $\lambda = 0.95$, $\kappa = 0.9$, $\chi_t = 0.4$, $T_{\Lambda_T} = 1.5 \text{ TeV}$, $T_\kappa = 700 \text{ GeV}$, $T_\lambda = -700 \text{ GeV}$ and $\sqrt{v_T^2 + \bar{v}_T^2} = 2 \text{ GeV}$. We employ the following parameters as variable parameters in the numerical analysis

$$M_2, \Lambda_T, \chi_d, A_t, T_{\chi_t}, T_{\chi_d}.$$

And in our next numerical analysis we keep the lightest chargino always more than 800 GeV, all the mass of sleptons and squarks are more than 1900 GeV.

A. The $h \rightarrow \gamma\gamma$, $h \rightarrow VV^*$ and $h \rightarrow Z\gamma$ in the TNMSSM

In this subsection we calculate the signal strengths for process $h \rightarrow \gamma\gamma$, $h \rightarrow VV^*$ and $h \rightarrow Z\gamma$. Some relevant formulas of $h \rightarrow \gamma\gamma$ and $h \rightarrow VV^*$ can be found in the works[27, 28]. At first we take parameters $M_2 = 1500 \text{ GeV}$, $\Lambda_T = 0.8$, $A_t = 1500 \text{ GeV}$

and $T_{\chi_d} = -800$ GeV. And we paint the signal strength of the $h \rightarrow \gamma\gamma$ varying with χ_d in Fig.3(a), for $T_{\chi_t} = -800$ GeV (solid line), $T_{\chi_t} = -900$ GeV (dashed line) and $T_{\chi_t} = -1000$ GeV (dot dashed line). In order to keep the SM-like Higgs mass satisfy the 3σ error of experimental constraints, we let the χ_d vary from 0.5 to 1. In Fig.3(a), all the three curves are $1.03 < \mu_{\gamma\gamma}^{ggF} < 1.16$ and they they behave the same way. These curves tend to be decreases with the increase of the χ_d . The solid line varies from 1.16 to 1.05, the dashed line varies from 1.15 to 1.045 and the dot dashed line varies from 1.14 to 1.035. Our results for process $h \rightarrow \gamma\gamma$ satisfy the experiment constraints[3].

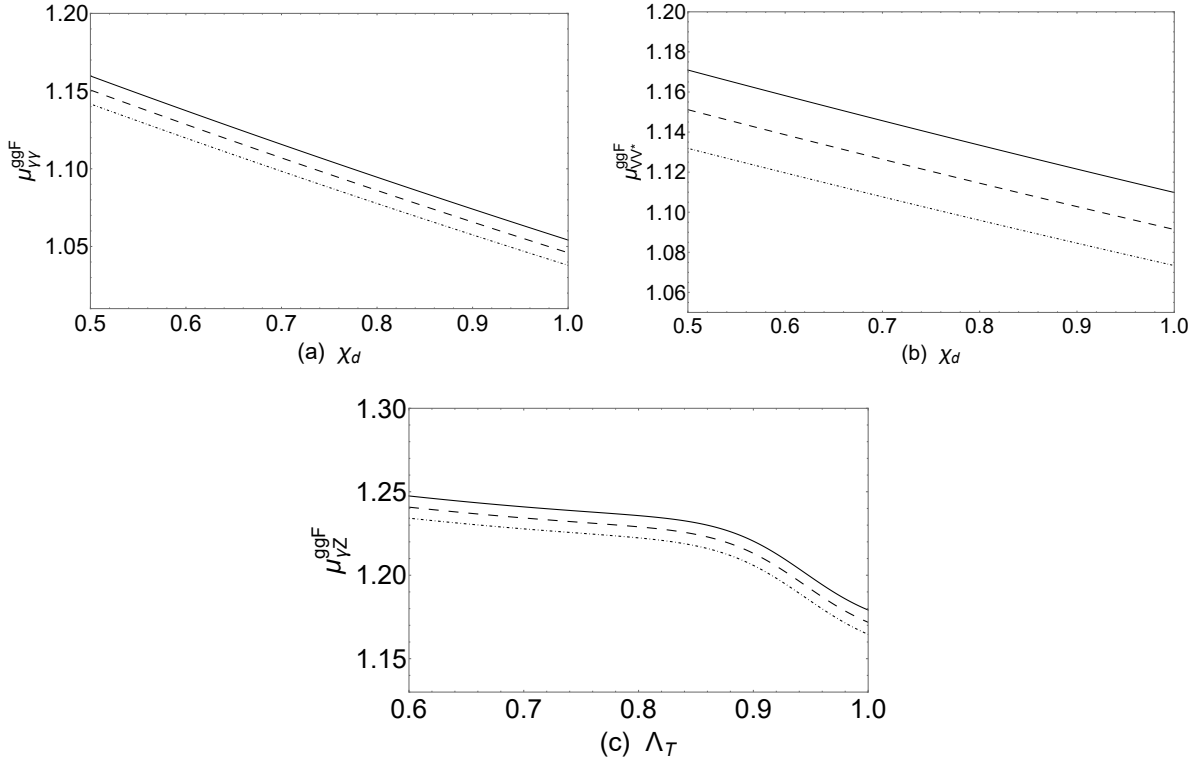


FIG. 3: (a) $\mu_{\gamma\gamma}^{ggF}$ varying with χ_d for $T_{\chi_t} = -800$ GeV (solid line), $T_{\chi_t} = -900$ GeV (dashed line) and $T_{\chi_t} = -1000$ GeV (dot dashed line). (b) μ_{VV}^{ggF} varying with χ_d for $\Lambda_T = 0.7$ (solid line), $\Lambda_T = 0.8$ (dashed line) and $\Lambda_T = 0.9$ (dot dashed line). (c) $\mu_{Z\gamma}^{ggF}$ varying with Λ_T for $\chi_d = 0.7$ (solid line), $\chi_d = 0.8$ (dashed line) and $\chi_d = 0.9$ (dot dashed line).

Then, the signal strengths for processes $h \rightarrow ZZ^*$ and $h \rightarrow WW^*$ are very close. So we take $\mu_{VV}^{ggF} = \mu_{WW}^{ggF} = \mu_{ZZ}^{ggF}$ for simplicity, and we just paint the signal strength of

$h \rightarrow ZZ^*$. We take parameters $M_2 = 1500$ GeV, $T_{\chi_d} = -800$ GeV, $T_{\chi_t} = -800$ GeV and $A_t = 1500$ GeV. And we paint the signal strength of the $h \rightarrow VV^*$ varying with χ_d in Fig.3(b), for $\Lambda_T = 0.7$ (solid line), $\Lambda_T = 0.8$ (dashed line) and $\Lambda_T = 0.9$ (dot dashed line). In Fig.3(b) the signal strength of the $h \rightarrow VV^*$ decreases with the increase of χ_d . These curves are above 1.073 and below 1.171, and their behaviors are similar to each other. The experiment constraints[3] $\mu_{ZZ^*}^{(exp)} = 1.01 \pm 0.07$, $\mu_{WW^*}^{(exp)} = 1.19 \pm 0.12$. So our calculate result $\mu_{ZZ^*}^{ggF}$ satisfies the experimental constraint that the error is 1σ , and $\mu_{WW^*}^{ggF}$ satisfies the experimental constraint that the error is 2σ .

The new physics contributions to the decay $h \rightarrow MZ$ come from the effective coupling of $hZ\gamma$. So we study the process $h \rightarrow Z\gamma$ at this subsection. In the numerical calculation of process $h \rightarrow Z\gamma$, we take the parameters $M_2 = 1500$ GeV, $T_{\chi_d} = -800$ GeV, $T_{\chi_t} = -800$ GeV and $A_t = 1500$ GeV. In Fig 3(c), these curves are close to each other. And all the curves are varies from 1.164 to 1.248. When $0.6 \leq \Lambda_T \leq 0.9$, all the lines here have a smaller slope. When $0.9 \leq \Lambda_T \leq 1$, all the lines here have a bigger slope. And the result agrees with the observed signal strength with 1.5σ .

B. The processes $h \rightarrow MZ$

In this subsection we will study the processes $h \rightarrow MZ$. The vector mesons decay constants for ω , ρ , ϕ , J/ψ and Υ can be found in Table I. The NP contribution of the process $h \rightarrow MZ$ comes from the effective coupling $hZ\gamma$. So our calculated results of decay $h \rightarrow MZ$ for different mesons should be similar.

Now we study the signal strengths of process $h \rightarrow MZ$. First, we take the parameter $T_{\chi_d} = -800$ GeV, $T_{\chi_t} = -800$ GeV and $A_t = 1500$ GeV. We paint the signal strengths of processes $h \rightarrow MZ$ in Fig.4. And in Fig.4 the solid line is obtained with $\chi_d = 0.7$, $\Lambda_T = 0.9$ the dashed line is obtained with $\chi_d = 0.8$, $\Lambda_T = 0.8$, and the dot dashed line is obtained with $\chi_d = 0.9$, $\Lambda_T = 0.7$. We can see from Fig.4 the signal strengths increase with the increase of M_2 at $1000 \text{ GeV} \leq M_2 \leq 1100 \text{ GeV}$, the signal strengths decrease with the increase of M_2 at $1100 \text{ GeV} \leq M_2 \leq 2000 \text{ GeV}$. The signal strengths of processes $h \rightarrow \omega Z$ are in region 1.18-1.223, the signal strengths of processes $h \rightarrow \rho Z$ are in region 1.183-1.235, the signal

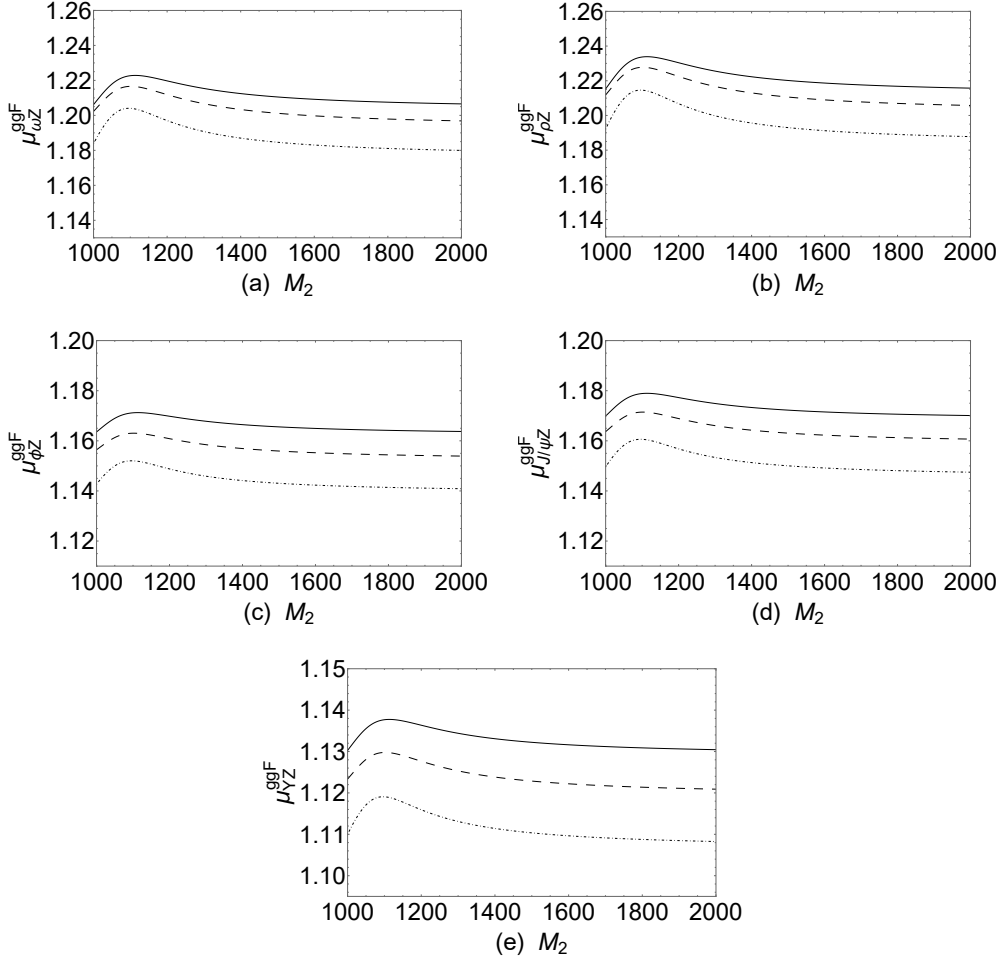


FIG. 4: The signal strengths versus M_2 are plotted by the the solid line ($\chi_d = 0.7, \Lambda_T = 0.9$), dashed line ($\chi_d = 0.8, \Lambda_T = 0.8$) and the dot dashed line ($\chi_d = 0.9, \Lambda_T = 0.7$), respectively.

strengths of processes $h \rightarrow \phi Z$ are in region 1.141-1.172, the signal strengths of processes $h \rightarrow J\psi Z$ are in region 1.147-1.179, the signal strengths of processes $h \rightarrow \Upsilon Z$ are in region 1.108-1.138.

The new contributions to the decay $h \rightarrow MZ$ come from the effective coupling of $h\gamma Z$. So we can infer that our results are consistent with the process $h \rightarrow \gamma Z$. As we can see, in Fig.3(c), the parameter Λ_T has obvious influence on signal strength $\mu_{Z\gamma}^{\text{ggF}}$. So we should research the signal strengths of processes $h \rightarrow MZ$ versus Λ_T . The parameters we take as $M_2 = 1500$ GeV, $T_{\chi_d} = -800$ GeV, $T_{\chi_t} = -800$ GeV and $A_t = 1500$ GeV. And in order to keep the Higgs mass satisfy the 3σ error of experimental constraints, the Λ_T is changed

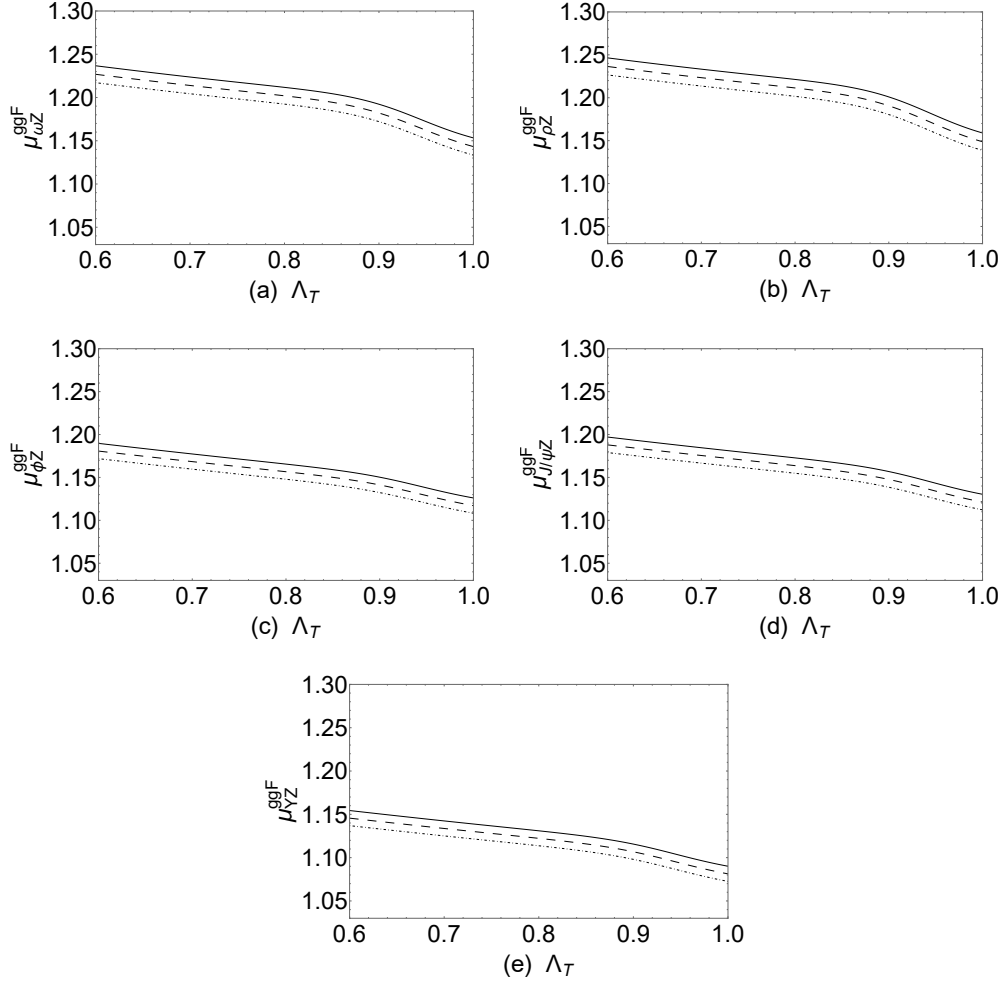


FIG. 5: The signal strengths versus Λ_T are plotted by the solid line ($\chi_d = 0.7$), dashed line ($\chi_d = 0.8$) and dot dashed line ($\chi_d = 0.9$), respectively.

from 0.6 to 1 with $\chi_d = 0.7, 0.8, 0.9$. The results for signal strengths of μ_{MZ}^{ggF} versus Λ_T are plotted in Fig. 5. The $\mu_{\omega Z}^{ggF}$ are in region 1.133-1.238, the $\mu_{\rho Z}^{ggF}$ are in region 1.138-1.249, the $\mu_{\phi Z}^{ggF}$ are in region 1.109-1.191, the $\mu_{J/\psi Z}^{ggF}$ are in region 1.112-1.198 and the $\mu_{\Upsilon Z}^{ggF}$ are in region 1.07-1.155. And we can see that the signal strengths of $h \rightarrow MZ$ are similar to the signal strength of $h \rightarrow Z\gamma$. In Fig.5, these solid lines all the curves are varies from 1.164 to 1.248. When $0.6 \leq \Lambda_T \leq 0.9$, all the lines here have a smaller slope. When $0.9 \leq \Lambda_T \leq 1$, all the lines here have a bigger slope. And we can see the signal strengths of $h \rightarrow MZ$ are decrease as χ_d increase.

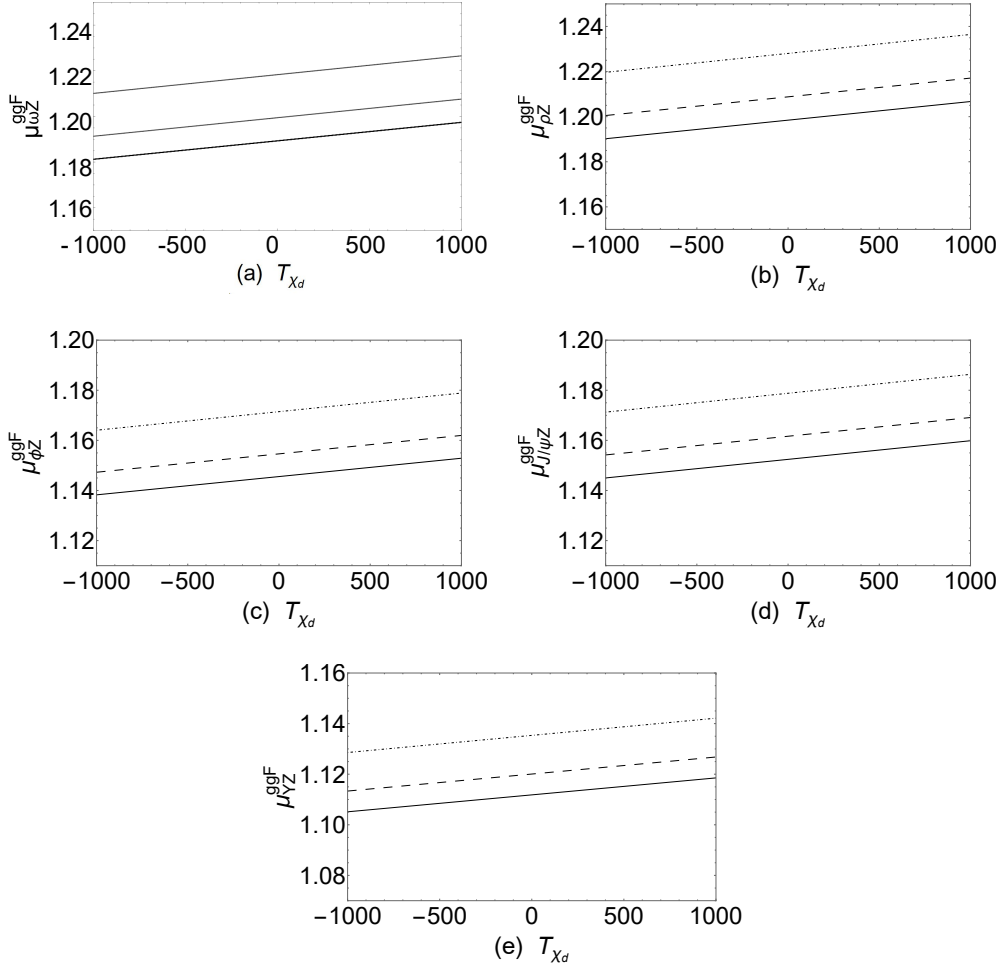


FIG. 6: The signal strengths versus T_{χ_d} are plotted by the solid line ($A_t = 1000$ GeV), dashed line ($A_t = 1200$ GeV) and dot dashed line ($A_t = 1500$ GeV).

Then we study the effect of the T_{χ_d} on signal strengths of $h \rightarrow MZ$. The parameters we take as $M_2 = 1500$ GeV, $\Lambda_T = 0.8$, $\chi_d = 0.7$ and $T_{\chi_t} = -800$ GeV. And in order to keep the SM-like Higgs mass satisfy the 3σ error of experimental constraints, we let the T_{χ_d} vary from -1000 GeV to 1000 GeV with $A_t = 1000, 1200, 1500$ GeV. We paint the signal strengths of processes $h \rightarrow MZ$ in Fig.6. And in Fig.6 the solid lines are obtained with $A_t = 1000$ GeV, the dashed lines are obtained with $A_t = 1200$ GeV and the dot dashed lines are obtained with $A_t = 1500$ GeV. In Fig.6, we can see tha the signal strengths increase with T_{χ_d} increase. In Fig.6(a) and Fig.6(b), the signal strength of the processes of the $h \rightarrow \omega Z$ and $h \rightarrow \rho Z$ are in region 1.181-1.227 and 1.19-1.237. In Fig.6(c) and Fig.6(d), the signal

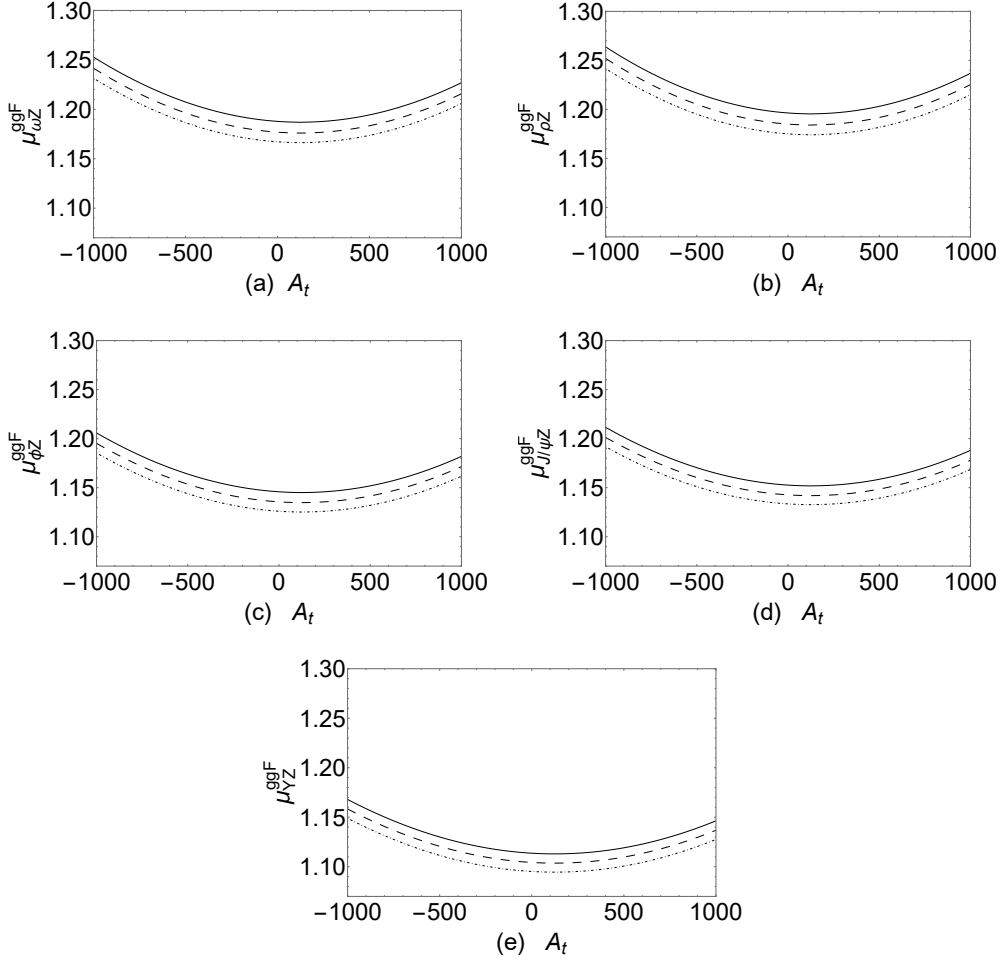


FIG. 7: The signal strengths versus A_t are plotted by the solid line ($\Lambda_T = 0.5$, $\chi_d = 0.8$), dashed line ($\Lambda_T = 0.6$, $\chi_d = 0.7$) and dot dashed line ($\Lambda_T = 0.7$, $\chi_d = 0.6$), respectively.

strength of processes $h \rightarrow \phi Z$ and $h \rightarrow J/\psi Z$ are region 1.138-1.178 and 1.145-1.186. The meson Υ is the heaviest meson we've studied. So that the signal strength of process $h \rightarrow \Upsilon Z$ is obviously less than the other results in Fig.6. The signal strength of process $h \rightarrow \Upsilon Z$ is in region 1.105-1.142. We can see from Fig.6, the A_t have a great influence on the signal strengths of $h \rightarrow MZ$. The signal strengths of $h \rightarrow MZ$ increase as the A_t increases.

At last we study the effect of the A_t on signal strengths of processes $h \rightarrow MZ$. The coupling of higgs and third generation squarks include the A_t . We take the parameters as $M_2 = 1500$ GeV, $T_{\chi_d} = -800$ GeV and $T_{\chi_t} = -800$ GeV. In order to keep the SM-like Higgs mass satisfy the 3σ error of experimental constrains, we let the A_t vary from -1000 GeV

to 1000 GeV with $(\Lambda_T = 0.5, \chi_d = 0.8)$, $(\Lambda_T = 0.6, \chi_d = 0.7)$ and $(\Lambda_T = 0.7, \chi_d = 0.6)$. We paint signal strengths of process $h \rightarrow MZ$ in Fig.7. In Fig.7 the solid lines are obtained with $\Lambda_T = 0.5, \chi_d = 0.8$, the dashed lines are obtained with $\Lambda_T = 0.6, \chi_d = 0.7$ and the dot dashed lines are obtained with $\Lambda_T = 0.7, \chi_d = 0.6$. In Fig.7(a) and Fig.7(b), the signal strengths of the processes $h \rightarrow \omega Z$ and $h \rightarrow \rho Z$ are in region 1.165-1.253 and 1.174-1.265. The signal strengths of processes $h \rightarrow \phi Z$ and $h \rightarrow J/\psi Z$ are in region 1.125-1.205 and 1.132-1.213. For the heaviest meson Υ we're studied, the signal strength of $h \rightarrow \Upsilon Z$ is obviously less than the other results in Fig.7. The lines in Fig.7(e) are in region 1.095-1.169.

V. CONCLUSION

In this work, we study the decays $h \rightarrow \gamma Z$ and $h \rightarrow MZ$ in the TNMSSM, with $M = \omega, \rho, \phi, J/\psi, \Upsilon$. There are two types of contributions to decay $h \rightarrow MZ$: the direct contributions and indirect contributions. For indirect contributions, there is a process $h \rightarrow Z\gamma^* \rightarrow MZ$, where γ^* is off-shell and changes into the final state vector meson. There is no $h\gamma Z$ coupling at tree level, but it can be contributed by loop diagram. In the models beyond SM, the coupling constant can be divided into two parts: CP-even coupling constant $C_{\gamma Z}$ and CP-odd coupling constant $\tilde{C}_{\gamma Z}$. The CP-even coupling constant $C_{\gamma Z}$ is more important than the CP-odd coupling constant $\tilde{C}_{\gamma Z}$.

The experiment results of the signal strengths $\mu_{\gamma\gamma}^{ggF}$ and μ_{ZZ}^{ggF} are $\mu_{\gamma\gamma}^{ggF} = 1.10 \pm 0.07$ and $\mu_{ZZ}^{ggF} = 1.01 \pm 0.07$. Our numerical results of the signal strengths $\mu_{\gamma\gamma}^{ggF}$ and μ_{ZZ}^{ggF} are in region 1.035-1.16 and 1.073-1.171 which satisfy the error of 1σ . Our numerical results of the signal strength in region 1.164-1.248. The result agrees with the observed signal strength with 1.5σ . The numerical results show that the TNMSSM contributions to the processes $h \rightarrow \omega Z$ and $h \rightarrow \rho Z$ are more considerable. The signal strengths $\mu_{\omega Z, \rho Z}^{ggF}$ are about 1.13-1.26. The TNMSSM corrections to the processes $h \rightarrow \phi Z$ and $h \rightarrow J/\psi Z$ are during 1.11-1.21, and $h \rightarrow \Upsilon Z$ about 1.07-1.17. The decays $h \rightarrow MZ$ may be accessible at future high energy colliders.

Acknowledgments

The work has been supported by the National Natural Science Foundation of China (NNSFC) with Grants No. 12075074, No. 12235008, Natural Science Foundation of Guangxi Autonomous Region with Grant No. 2022GXNSFDA035068, Hebei Natural Science Foundation with Grant No. A2022201017, No. A2023201041, the youth top-notch talent support program of the Hebei Province.

Appendix A: Form factors

The form factors are

$$A_0(\tau, \lambda) = I_1(\tau, \lambda), \quad (\text{A1})$$

$$A_{1/2}(\tau, \lambda) = I_1(\tau, \lambda) - I_2(\tau, \lambda) \quad (\text{A2})$$

with

$$I_1(\tau, \lambda) = \frac{\tau\lambda}{2(\tau - \lambda)} + \frac{\tau^2\lambda^2}{2(\tau - \lambda)^2}[f(\tau^{-1}) - f(\lambda^{-1})] + \frac{\tau^2\lambda}{(\tau - \lambda)^2}[g(\tau^{-1}) - g(\lambda^{-1})] \quad (\text{A3})$$

$$I_2(\tau, \lambda) = -\frac{\tau\lambda}{2(\tau - \lambda)}[f(\tau^{-1}) - f(\lambda^{-1})] \quad (\text{A4})$$

the $f(x)$ and $g(x)$ are here:

$$f(x) = \begin{cases} \arcsin^2 \sqrt{x}, & x \leq 1 \\ -\frac{1}{4} \left[\ln \frac{1+\sqrt{1-1/x}}{1-\sqrt{1-1/x}} - i\pi \right]^2, & x > 1 \end{cases} \quad (\text{A5})$$

$$g(x) = \begin{cases} \sqrt{x^{-1} - 1} \arcsin \sqrt{x}, & x \geq 1 \\ \frac{\sqrt{1-x^{-1}}}{2} \left[\ln \frac{1+\sqrt{1-1/x}}{1-\sqrt{1-1/x}} - i\pi \right], & x < 1 \end{cases} \quad (\text{A6})$$

Appendix B: The mass of Higgs and Charginos

In the basis $(\phi_d, \phi_u, \phi_s, \phi_T, \phi_{\bar{T}})$, the definition of mass squared matrix for neutral Higgs is given by

$$m_h^2 = \begin{pmatrix} m_{\phi_d\phi_d} & m_{\phi_u\phi_d} & m_{\phi_s\phi_d} & m_{\phi_T\phi_d} & m_{\phi_{\bar{T}}\phi_d} \\ m_{\phi_d\phi_u} & m_{\phi_u\phi_u} & m_{\phi_s\phi_u} & m_{\phi_T\phi_u} & m_{\phi_{\bar{T}}\phi_u} \\ m_{\phi_d\phi_s} & m_{\phi_u\phi_s} & m_{\phi_s\phi_s} & m_{\phi_T\phi_s} & m_{\phi_{\bar{T}}\phi_s} \\ m_{\phi_d\phi_T} & m_{\phi_u\phi_T} & m_{\phi_s\phi_T} & m_{\phi_T\phi_T} & m_{\phi_{\bar{T}}\phi_T} \\ m_{\phi_d\phi_{\bar{T}}} & m_{\phi_u\phi_{\bar{T}}} & m_{\phi_s\phi_{\bar{T}}} & m_{\phi_T\phi_{\bar{T}}} & m_{\phi_{\bar{T}}\phi_{\bar{T}}} \end{pmatrix} \quad (\text{B1})$$

where

$$m_{\phi_d\phi_d} = m_{H_d}^2 + \frac{1}{8}(g_1^2 + g_2^2)(2v_{\bar{T}}^2 - 2v_T^2 + 3v_d^2 - v_u^2) + \sqrt{2}v_T\Re(T_{\chi_d}) + \frac{|\lambda|^2}{2}(v_s^2 + v_u^2) - v_s v_{\bar{T}}\Re(\chi_d\Lambda_T^*) + (3v_d^2 + 2v_{\bar{T}}^2)|\chi_d|^2, \quad (\text{B2})$$

$$m_{\phi_d\phi_u} = -\frac{1}{4}(g_1^2 + g_2^2)v_d v_u - \frac{1}{\sqrt{2}}v_s\Re(T_\lambda) + \frac{1}{2}v_T v_{\bar{T}}\Re(\lambda\Lambda_T^*) + v_d v_u |\lambda|^2 - v_s v_{\bar{T}}\Re(\chi_t\lambda^*) - v_s v_T\Re(\chi_d\lambda^*) - \frac{1}{2}v_s^2\Re(\kappa\lambda^*), \quad (\text{B3})$$

$$m_{\phi_u\phi_u} = m_{H_u}^2 - \frac{1}{8}(g_1^2 + g_2^2)(2v_{\bar{T}}^2 - 2v_T^2 - 3v_u^2 + v_d^2) + \sqrt{2}v_{\bar{T}}\Re(T_{\chi_t}) + \frac{1}{2}(v_d^2 + v_s^2)|\lambda|^2 - v_s v_T\Re(\chi_t\Lambda_T^*) + (2v_{\bar{T}}^2 + 3v_u^2)|\chi_t|^2, \quad (\text{B4})$$

$$m_{\phi_d\phi_s} = v_d v_s |\lambda|^2 - \frac{1}{\sqrt{2}}v_u\Re(T_\lambda) - v_s v_u\Re(\kappa\lambda^*) - v_T v_u\Re(\lambda\chi_d^*) - v_{\bar{T}}v_u\Re(\chi_t\lambda^*) - v_d v_{\bar{T}}\Re(\Lambda_T\chi_d^*), \quad (\text{B5})$$

$$m_{\phi_u\phi_s} = v_s v_u |\lambda|^2 - \frac{1}{\sqrt{2}}v_d\Re(T_\lambda) - v_d v_s\Re(\lambda\kappa^*) - v_T v_d\Re(\lambda\chi_d^*) - v_d v_{\bar{T}}\Re(\lambda\chi_t^*) - v_T v_u\Re(\chi_t\Lambda_T^*), \quad (\text{B6})$$

$$m_{\phi_s\phi_s} = m_S^2 + \frac{|\Lambda_T|^2}{2}(v_T^2 + v_{\bar{T}}^2) - v_T v_{\bar{T}}\Re(\kappa\Lambda_T^*) + 3v_s^2|\kappa|^2 - v_d v_u\Re(\lambda\kappa^*) + \frac{1}{2}(v_d^2 + v_u^2)|\lambda|^2 + \sqrt{2}v_s\Re(T_\kappa), \quad (\text{B7})$$

$$m_{\phi_d\phi_T} = -\frac{1}{2}(g_1^2 + g_2^2)v_d v_u + \frac{1}{2}v_u v_{\bar{T}}\Re(\lambda\Lambda_T^*) - v_u v_s\Re(\lambda\chi_d^*) + 4v_d v_T |\chi_d|^2 + \sqrt{2}v_d\Re(T_{\chi_d}), \quad (\text{B8})$$

$$m_{\phi_u\phi_T} = \frac{1}{2}(g_1^2 + g_2^2)v_d v_T - v_u v_s\Re(\Lambda_T\chi_t^*) - v_d v_s\Re(\lambda\chi_d^*) + \frac{1}{2}v_d v_{\bar{T}}\Re(\lambda\Lambda_T^*), \quad (\text{B9})$$

$$m_{\phi_s\phi_T} = v_s v_T |\lambda|^2 - \frac{1}{\sqrt{2}} v_{\bar{T}} \Re(T_\Lambda) - v_s v_{\bar{T}} \Re(\kappa \Lambda_T^*) - v_d v_u \Re(\lambda \chi_d^*) - \frac{1}{2} v_u^2 \Re(\chi_t \Lambda_T^*), \quad (\text{B10})$$

$$m_{\phi_T\phi_T} = m_T^2 - \frac{1}{4} (g_1^2 + g_2^2) (2v_T^2 - 6v_T^2 - v_u^2 + v_d^2) + 2v_d^2 |\chi_d|^2 + \frac{1}{2} (v_s^2 + v_{\bar{T}}^2) |\Lambda_T|^2, \quad (\text{B11})$$

$$m_{\phi_d\phi_{\bar{T}}} = \frac{1}{2} (g_1^2 + g_2^2) v_d v_{\bar{T}} + \frac{1}{2} v_T v_u \Re(\lambda \Lambda_T^*) - v_d v_s \Re(\chi_d \Lambda_T^*) - v_s v_u \Re(\chi_t \lambda^*), \quad (\text{B12})$$

$$m_{\phi_u\phi_{\bar{T}}} = -\frac{1}{2} (g_1^2 + g_2^2) v_{\bar{T}} v_u + \sqrt{2} v_u \Re(T_{\chi_t}) + \frac{1}{2} v_d v_T \Re(\lambda \Lambda_T^*) - v_d v_s \Re(\lambda \chi_t^*) + 4v_{\bar{T}} v_u |\chi_t|^2, \quad (\text{B13})$$

$$m_{\phi_s\phi_{\bar{T}}} = v_s v_{\bar{T}} |\Lambda_T|^2 - \frac{1}{\sqrt{2}} v_T \Re(T_\Lambda) - v_s v_T \Re(\kappa \Lambda_T^*) - \frac{1}{2} v_d^2 \Re(\Lambda_T \chi_d^*) - v_d v_u \Re(\lambda \chi_t^*), \quad (\text{B14})$$

$$m_{\phi_T\phi_{\bar{T}}} = -(g_1^2 + g_2^2) v_T v_{\bar{T}} - \frac{1}{\sqrt{2}} v_s \Re(T_\Lambda) - \frac{1}{2} v_s^2 \Re(\kappa \Lambda_T^*) + \frac{1}{2} v_d v_u \Re(\lambda \Lambda_T^*) + v_T v_{\bar{T}} |\Lambda_T|^2, \quad (\text{B15})$$

$$m_{\phi_{\bar{T}}\phi_{\bar{T}}} = m_{\bar{T}}^2 + \frac{1}{4} (g_1^2 + g_2^2) (v_d^2 - v_u^2 - 2v_T^2 + 6v_{\bar{T}}^2) + \frac{1}{2} (v_s^2 + v_T^2) |\Lambda_T|^2 + 2v_u^2 |\chi_t|^2. \quad (\text{B16})$$

This matrix is diagonalized by Z^H :

$$Z^H m_h^2 Z^{H\dagger} = m_{2,h}^{\text{dia}}$$

with

$$\phi_d = \sum_j Z_{j1}^H h_j, \quad \phi_u = \sum_j Z_{j2}^H h_j, \quad \phi_s = \sum_j Z_{j3}^H h_j, \quad \phi_T = \sum_j Z_{j4}^H h_j, \quad \phi_{\bar{T}} = \sum_j Z_{j5}^H h_j.$$

In the basis $(\tilde{W}^-, \tilde{H}_d^-, \tilde{T}^-)$, $(\tilde{W}^+, \tilde{H}_u^+, \tilde{T}^+)$, the definition of mass matrix for charginos is given by

$$m_{\tilde{\chi}^-} = \begin{pmatrix} M_2 & \frac{1}{\sqrt{2}} g_2 v_u & g_2 v_T \\ \frac{1}{\sqrt{2}} g_2 v_d & \frac{1}{\sqrt{2}} v_s \lambda & -v_d \chi_d \\ g_2 v_{\bar{T}} & -v_u \chi_t & \frac{1}{\sqrt{2}} \Lambda_T v_s \end{pmatrix} \quad (\text{B17})$$

This matrix is diagonalized by U and V

$$U^* m_{\tilde{\chi}^-} V^\dagger = m_{\tilde{\chi}^-}^{\text{dia}}$$

with

$$\begin{aligned} \tilde{W}^- &= \sum_j U_{j1}^* \lambda_j^-, & \tilde{H}_d^- &= \sum_j U_{j2}^* \lambda_j^-, & \tilde{T}^- &= \sum_j U_{j3}^* \lambda_j^- \\ \tilde{W}^+ &= \sum_j V_{1j}^* \lambda_j^+, & \tilde{H}_u^+ &= \sum_j V_{2j}^* \lambda_j^+, & \tilde{T}^+ &= \sum_j V_{3j}^* \lambda_j^+ \end{aligned}$$

Appendix C: Tadpole equation and some corresponding vertexes

The CP-even tree level part of tadpole are given by

$$\begin{aligned}
\frac{\partial V}{\partial \phi_d} = & +\frac{1}{8}(g_1^2 + g_2^2)v_d(2v_{\bar{T}}^2 - 2v_T^2 - v_u^2 + v_d^2) + \frac{1}{4}\left(v_{\bar{T}}\left(\left(-2v_d v_s \chi_d + v_T v_u \lambda\right)\Lambda_T^* \right. \right. \\
& \left. \left. - 2v_s v_u \lambda \chi_t^*\right) - v_s^2 v_u \lambda \kappa^* + \left(2v_d(v_s^2 + v_u^2)\lambda + v_u\left(\Lambda_T v_T v_{\bar{T}} - v_s\left(2(v_{\bar{T}}\chi_t + v_T\chi_d) + v_s\kappa\right)\right)\right)\lambda^* \right. \\
& \left. + 4v_d\left(\sqrt{2}v_T\Re(T_{\chi_d}) + m_{H_d}^2\right) \right. \\
& \left. - 2\left(\sqrt{2}v_s v_u \Re(T_\lambda) + \left(v_d\left(-2(2v_T^2 + v_d^2)\chi_d + \Lambda_T v_s v_{\bar{T}}\right) + v_s v_T v_u \lambda\right)\chi_d^*\right)\right) \quad (C1)
\end{aligned}$$

$$\begin{aligned}
\frac{\partial V}{\partial \phi_u} = & +\frac{1}{8}(g_1^2 + g_2^2)v_u\left(-2v_{\bar{T}}^2 + 2v_T^2 - v_d^2 + v_u^2\right) \\
& + \frac{1}{4}\left(\left(4v_u^3 + 8v_{\bar{T}}^2 v_u\right)|\chi_t|^2 + v_T\left(-2v_d v_s \lambda \chi_d^* + \left(-2v_s v_u \chi_t + v_d v_{\bar{T}}\lambda\right)\Lambda_T^*\right) \right. \\
& \left. + \left(2\left(v_d^2 + v_s^2\right)v_u \lambda + v_d\left(\Lambda_T v_T v_{\bar{T}} - v_s\left(2(v_{\bar{T}}\chi_t + v_T\chi_d) + v_s\kappa\right)\right)\right)\lambda^* \right. \\
& \left. + v_u\left(-2\Lambda_T v_s v_T \chi_t^* + 4\left(\sqrt{2}v_{\bar{T}}\Re(T_{\chi_t}) + m_{H_u}^2\right)\right) \right. \\
& \left. + v_d\left(-2\sqrt{2}v_s \Re(T_\lambda) + \lambda\left(-2v_s v_{\bar{T}}\chi_t^* - v_s^2 \kappa^*\right)\right)\right) \quad (C2)
\end{aligned}$$

$$\begin{aligned}
\frac{\partial V}{\partial \phi_s} = & \frac{1}{4}\left(\left(-v_d^2 v_{\bar{T}}\chi_d + v_s\left(2\Lambda_T\left(v_T^2 + v_{\bar{T}}^2\right) - 2v_T v_{\bar{T}}\kappa\right) - v_T v_u^2 \chi_t\right)\Lambda_T^* + \left(-2v_d v_T v_u \lambda - \Lambda_T v_d^2 v_{\bar{T}}\right)\chi_d^* \right. \\
& \left. + \left(-2v_d v_{\bar{T}} v_u \lambda - \Lambda_T v_T v_u^2\right)\chi_t^* + \left(-2v_d v_s v_u \lambda + 4v_s^3 \kappa\right)\kappa^* + v_s\left(-2\Lambda_T v_T v_{\bar{T}}\kappa^* + 4m_S^2\right) \right. \\
& \left. + 2\left(-v_d v_u\left(v_{\bar{T}}\chi_t + v_s\kappa + v_T\chi_d\right) + v_s\left(v_d^2 + v_u^2\right)\lambda\right)\lambda^* \right. \\
& \left. + \sqrt{2}\left(-2v_d v_u \Re(T_\lambda) - 2v_T v_{\bar{T}}\Re(T_{\Lambda_T}) + v_s^2\left(T_\kappa^* + T_\kappa\right)\right)\right) \quad (C3)
\end{aligned}$$

$$\begin{aligned}
\frac{\partial V}{\partial \phi_T} = & +\frac{1}{4}(g_1^2 + g_2^2)v_T\left(-2v_{\bar{T}}^2 + 2v_T^2 - v_d^2 + v_u^2\right) \\
& + \frac{1}{4}\left(4m_T^2 v_T + \left(2\Lambda_T v_T\left(v_s^2 + v_{\bar{T}}^2\right) + v_d v_{\bar{T}} v_u \lambda - v_s\left(v_s v_{\bar{T}}\kappa + v_u^2 \chi_t\right)\right)\Lambda_T^* \right. \\
& \left. + \Lambda_T\left(-v_s^2 v_{\bar{T}}\kappa^* - v_s v_u^2 \chi_t^*\right) + v_d\left(2\left(4v_d v_T \chi_d - v_s v_u \lambda\right)\chi_d^* + v_u\left(-2v_s \chi_d + \Lambda_T v_{\bar{T}}\right)\lambda^*\right) \right. \\
& \left. - 2\sqrt{2}v_s v_{\bar{T}}\Re(T_{\Lambda_T}) + 2\sqrt{2}v_d^2 \Re(T_{\chi_d})\right) \quad (C4)
\end{aligned}$$

$$\begin{aligned}
\frac{\partial V}{\partial \phi_{\bar{T}}} = & +\frac{1}{4}(g_1^2 + g_2^2)v_{\bar{T}}\left(2v_{\bar{T}}^2 - 2v_T^2 - v_u^2 + v_d^2\right) \\
& + \frac{1}{4}\left(4v_{\bar{T}}\left(2v_u^2 |\chi_t|^2 + m_{\bar{T}}^2\right) + \left(2\Lambda_T\left(v_s^2 + v_{\bar{T}}^2\right)v_{\bar{T}} + v_d v_T v_u \lambda - v_s\left(v_d^2 \chi_d + v_s v_T \kappa\right)\right)\Lambda_T^* \right. \\
& \left. - \Lambda_T v_s^2 v_T \kappa^* + v_d v_u\left(-2v_s \chi_t + \Lambda_T v_T\right)\lambda^* + v_s\left(-2\left(\sqrt{2}v_T \Re(T_{\Lambda_T}) + v_d v_u \lambda \chi_t^*\right) - \Lambda_T v_d^2 \chi_d^*\right) \right. \\
& \left. + \sqrt{2}v_u^2\left(T_{\chi_t^*} + T_{\chi_t}\right)\right) \quad (C5)
\end{aligned}$$

Then we can identify the $m_{H_d}^2$, $m_{H_u}^2$, m_S^2 , m_T^2 and $m_{\bar{T}}^2$ by the minimum conditions of the scalar potential.

Here, we show some corresponding vertexes in this model. Their concrete forms are shown as

$$C_{Z\chi_i^+\chi_j^-}^L = \frac{1}{2}(-2g_1 \sin \theta_W U_{j3}^* U_{i3} + 2g_2 \cos \theta_W U_{j1}^* U_{i1} + (-g_1 \sin \theta_W + g_2 \cos \theta_W) U_{j2}^* U_{i2}) \quad (C6)$$

$$C_{Z\chi_i^+\chi_j^-}^R = \frac{1}{2}(-2g_1 \sin \theta_W V_{j3}^* V_{i3} + 2g_2 \cos \theta_W V_{j1}^* V_{i1} + (-g_1 \sin \theta_W + g_2 \cos \theta_W) V_{j2}^* V_{i2}) \quad (C7)$$

$$C_{Z\chi^{++}\chi^{--}}^L = C_{h\chi^{++}\chi^{--}}^R = (-g_1 \sin \theta_W + g_2 \cos \theta_W) \quad (C8)$$

$$C_{h_k\chi_i^+\chi_j^-}^L = -\frac{1}{2}[g_2 U_{j1}^*(2V_{i3}^* Z_{k4}^H + \sqrt{2}V_{i2}^* Z_{k2}^H) + U_{j2}^*(-2\chi_d V_{i3}^* Z_{k1}^H + \sqrt{2}g_2 V_{i1}^* Z_{k3}^H + \sqrt{2}\lambda V_{i2}^* Z_{k3}^H) + U_{j3}^*(-2\chi_t V_{i2}^* Z_{k2}^H + 2g_2 V_{i1}^* Z_{k5}^H + \sqrt{2}\Lambda_T V_{i3}^* Z_{k3}^H)] \quad (C9)$$

$$C_{h_k\chi_i^+\chi_j^-}^R = -\frac{1}{2}[g_2 U_{i1}(2V_{j3} Z_{k4}^H + \sqrt{2}V_{j2} Z_{k2}^H) + U_{i2}(-2\chi_d^* V_{j3} Z_{k1}^H + \sqrt{2}g_2 V_{j1} Z_{k3}^H + \sqrt{2}\lambda^* V_{j2} Z_{k3}^H) + U_{i3}(-2\chi_t^* V_{j2} Z_{k2}^H + 2g_2 V_{j1} Z_{k5}^H + \sqrt{2}\Lambda_T^* V_{j3} Z_{k3}^H)] \quad (C10)$$

$$C_{h_k\chi^{++}\chi^{--}}^L = \frac{1}{\sqrt{2}}\Lambda_T Z_{k3}^H \quad (C11)$$

$$C_{h_k\chi^{++}\chi^{--}}^R = \frac{1}{\sqrt{2}}\Lambda_T^* Z_{k3}^H \quad (C12)$$

For the coupling between Higgs particles and charged scalar particles is too complicated, we calculate it by computer.

$$V_{\text{scalar}} = W_i^* W^i + \frac{1}{2} \sum_a g_2^2 [H_u^\dagger \frac{\sigma^a}{2} H_u + H_d^\dagger \frac{\sigma^a}{2} H_d + Tr(T^\dagger \sigma^a T) + Tr(\bar{T}^\dagger \sigma^a \bar{T})]^2 + g_1^2 [\frac{1}{2} H_u^\dagger H_u - \frac{1}{2} H_d^\dagger H_d + T^\dagger T - \bar{T}^\dagger \bar{T} + \frac{1}{6} \tilde{Q}^\dagger \tilde{Q} - \frac{1}{2} \tilde{L}^\dagger \tilde{L} - \frac{2}{3} \tilde{u}_R^* \tilde{u}_R + \frac{1}{3} \tilde{d}_R^* \tilde{d}_R + \tilde{e}_R^* \tilde{e}_R + Tr(T^\dagger T) - Tr(\bar{T}^\dagger \bar{T})]^2 + V_{\text{soft}}$$

where $W_i = \frac{\partial W}{\partial \phi_i}$. And the coefficient C are as follow:

$$C_{h_k\phi_i\phi_j} = \frac{\partial^3 V_{\text{scalar}}}{\partial h_k \partial \phi_i \partial \phi_j} \Big|_{\langle H_{d,u}^0 \rangle = \frac{v_{d,u}}{\sqrt{2}}, \langle S \rangle = \frac{v_s}{\sqrt{2}}, \langle T \rangle = \frac{v_T}{\sqrt{2}}, \langle \bar{T} \rangle = \frac{v_{\bar{T}}}{\sqrt{2}}, \langle \text{the other fields} \rangle = 0} \quad (C13)$$

where ϕ_i represent the scalar field: H^\pm , $H^{\pm\pm}$, \tilde{u}_L , \tilde{u}_R , \tilde{d}_L , \tilde{d}_R , \tilde{e}_L and \tilde{e}_R .

[1] G. Aad et al. (ATLAS Collaboration), *Phys. Lett.* **B 716** (2012) 1.

- [2] S. Chatrchyan et al. (CMS Collaboration), *Phys. Lett. B* **716** (2012) 30.
- [3] R. L. Workman *et al.* [Particle Data Group], *PTEP* **2022**, 083C01 (2022)
doi:10.1093/ptep/ptac097
- [4] S. Weinberg, *Phys. Rev. D* **13**, 974-996 (1976) doi:10.1103/PhysRevD.19.1277
- [5] L. Susskind, *Phys. Rev. D* **20**, 2619-2625 (1979) doi:10.1103/PhysRevD.20.2619
- [6] U. Ellwanger and C. Hugonie, *Mod. Phys. Lett. A* **22**, 1581-1590 (2007)
doi:10.1142/S0217732307023870 [arXiv:hep-ph/0612133 [hep-ph]].
- [7] B. Ananthanarayan and P. N. Pandita, *Phys. Lett. B* **371**, 245-251 (1996) doi:10.1016/0370-2693(96)00010-X [arXiv:hep-ph/9511415 [hep-ph]].
- [8] B. Ananthanarayan and P. N. Pandita, *Int. J. Mod. Phys. A* **12**, 2321-2342 (1997)
doi:10.1142/S0217751X97001353 [arXiv:hep-ph/9601372 [hep-ph]].
- [9] J. D. Mason, *Phys. Rev. D* **80**, 015026 (2009) doi:10.1103/PhysRevD.80.015026
[arXiv:0904.4485 [hep-ph]].
- [10] K. Agashe, A. Azatov, A. Katz and D. Kim, *Phys. Rev. D* **84**, 115024 (2011)
doi:10.1103/PhysRevD.84.115024 [arXiv:1109.2842 [hep-ph]].
- [11] J. R. Espinosa and M. Quiros, *Phys. Lett. B* **279**, 92-97 (1992) doi:10.1016/0370-2693(92)91846-2
- [12] J. R. Espinosa and M. Quiros, *Phys. Lett. B* **302**, 51-58 (1993) doi:10.1016/0370-2693(93)90634-T [arXiv:hep-ph/9212305 [hep-ph]].
- [13] J. R. Espinosa and M. Quiros, *Phys. Rev. Lett.* **81**, 516-519 (1998)
doi:10.1103/PhysRevLett.81.516 [arXiv:hep-ph/9804235 [hep-ph]].
- [14] M. Gonzalez-Alonso and G. Isidori, *Phys. Lett. B* **733**, 359-365 (2014)
doi:10.1016/j.physletb.2014.05.004 [arXiv:1403.2648 [hep-ph]].
- [15] G. Isidori, A. V. Manohar and M. Trott, *Phys. Lett. B* **728**, 131-135 (2014)
doi:10.1016/j.physletb.2013.11.054 [arXiv:1305.0663 [hep-ph]].
- [16] S. Alte, M. König and M. Neubert, *JHEP* **12**, 037 (2016) doi:10.1007/JHEP12(2016)037
[arXiv:1609.06310 [hep-ph]].
- [17] S. M. Zhao, T. F. Feng, J. B. Chen, J. J. Feng, G. Z. Ning and H. B. Zhang, *Phys. Rev. D* **97**, no.9, 095043 (2018) doi:10.1103/PhysRevD.97.095043 [arXiv:1805.05048 [hep-ph]].

- [18] A. L. Kagan, G. Perez, F. Petriello, Y. Soreq, S. Stoynev and J. Zupan, Phys. Rev. Lett. **114**, no.10, 101802 (2015) doi:10.1103/PhysRevLett.114.101802 [arXiv:1406.1722 [hep-ph]].
- [19] G. T. Bodwin, H. S. Chung, J. H. Ee, J. Lee and F. Petriello, Phys. Rev. D **90**, no.11, 113010 (2014) doi:10.1103/PhysRevD.90.113010 [arXiv:1407.6695 [hep-ph]].
- [20] G. Aad *et al.* [ATLAS], JHEP **10**, 013 (2021) doi:10.1007/JHEP10(2021)013 [arXiv:2104.13240 [hep-ex]].
- [21] G. Aad *et al.* [ATLAS and CMS], Phys. Rev. Lett. **132**, no.2, 021803 (2024) doi:10.1103/PhysRevLett.132.021803 [arXiv:2309.03501 [hep-ex]].
- [22] L. Bergstrom and G. Hulth, Nucl. Phys. B **259**, 137-155 (1985) [erratum: Nucl. Phys. B **276**, 744-744 (1986)] doi:10.1016/0550-3213(85)90302-5
- [23] M. Spira, A. Djouadi and P. M. Zerwas, Phys. Lett. B **276**, 350-353 (1992) doi:10.1016/0370-2693(92)90331-W
- [24] V. L. Chernyak and A. R. Zhitnitsky, Nucl. Phys. B **201**, 492 (1982) [erratum: Nucl. Phys. B **214**, 547 (1983)] doi:10.1016/0550-3213(83)90251-1
- [25] N. H. Fuchs and M. D. Scadron, Phys. Rev. D **20**, 2421 (1979) doi:10.1103/PhysRevD.20.2421
- [26] M. Beneke, G. Buchalla, M. Neubert and C. T. Sachrajda, Nucl. Phys. B **591**, 313-418 (2000) doi:10.1016/S0550-3213(00)00559-9 [arXiv:hep-ph/0006124 [hep-ph]].
- [27] A. Djouadi, Phys. Rept. **457**, 1-216 (2008) doi:10.1016/j.physrep.2007.10.004 [arXiv:hep-ph/0503172 [hep-ph]].
- [28] A. Djouadi, Phys. Rept. **459**, 1-241 (2008) doi:10.1016/j.physrep.2007.10.005 [arXiv:hep-ph/0503173 [hep-ph]].